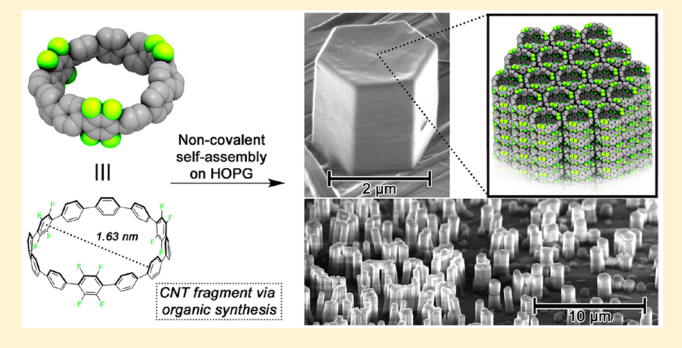
IV II VOLETTERS

A Bottom-Up Approach to Solution-Processed, Atomically Precise Graphitic Cylinders on Graphite

Erik J. Leonhardt, Jeff M. Van Raden, David Miller, Lev N. Zakharov, Benjamín Alemán, And Ramesh Jasti

Supporting Information

ABSTRACT: Extended carbon nanostructures, such as carbon nanotubes (CNTs), exhibit remarkable properties but are difficult to synthesize uniformly. Herein, we present a new class of carbon nanomaterials constructed via the bottom-up self-assembly of cylindrical, atomically precise small molecules. Guided by supramolecular design principles and circle packing theory, we have designed and synthesized a fluorinated nanohoop that, in the solid state, self-assembles into nanotube-like arrays with channel diameters of precisely 1.63 nm. A mild solution-casting technique is then used to construct vertical "forests" of these arrays on a highly ordered pyrolytic graphite (HOPG) surface through epitaxial growth.



Furthermore, we show that a basic property of nanohoops, fluorescence, is readily transferred to the bulk phase, implying that the properties of these materials can be directly altered via precise functionalization of their nanohoop building blocks. The strategy presented is expected to have broader applications in the development of new graphitic nanomaterials with π -rich cavities reminiscent of CNTs.

KEYWORDS: Cycloparaphenylene, nanohoop, carbon nanotube, self-assembly, epitaxial growth, vertical alignment

arbon nanotubes (CNTs) exhibit a wide range of unique properties depending on their precise atomic structure. The remarkable optical and electronic properties of CNTs are intimately connected to CNT chirality.1 The scalable preparation of single-chirality CNTs, therefore, has been a longstanding goal in the field of nanoscience.^{2–4} Similarly, the unique frictionless channels of CNTs exhibit fascinating mass transport behavior, but only when the channel diameters are smaller than 2 nm,^{5,6} again highlighting the need for precise CNT structural control. In addition to chirality and diameter, the position and orientation of CNTs on substrates (for example, the vertical alignment of CNTs into surface-bound "forests")⁷ is important for fully realizing potential applications such as membranes, sensors, and electronics. While much progress has been made in the synthesis and deposition of CNTs, a completely new approach to these types of cylindrical materials may open up new opportunities. Herein, we disclose a "bottom-up" synthesis strategy based on selfassembly of short fragments of CNTs (i.e., cycloparaphenylenes or carbon nanohoops, Figure 1a) to produce vertically oriented "forests" of graphitic cylinders on surfaces with precise structural control.

Inspired by the work of Smalley regarding the amplification of CNTs, 12 the synthesis of cycloparaphenylenes (CPPs) aimed to provide ideal templates or building blocks for the uniform fabrication of CNTs. 13-15 Since their initial synthesis in 2008, 16 methods have been developed to synthesize these "carbon nanohoops" in various sizes ^{17–20} and with numerous functionalities. ^{21–23} More recently, "carbon nanobelts" have been synthesized by Itami and co-workers, again in hopes of accessing effective seed molecules for CNT growth. 24,25 As a consequence of their curved geometries and cyclic conjugation, carbon nanohoops and nanobelts exhibit unique size-dependent electronic and photophysical properties. 24-27 Despite their fascinating circular geometries, CNT-like pores, and highly tunable properties, CPPs and related structures have only recently begun to be explored in the context of solid-state materials. 28-32 Seeking to expand on this, we envisioned the development of a new class of CPP-based carbon nanomaterials that would mimic the tubular structures of CNTs.

Received: October 3, 2018
Revised: November 20, 2018
Published: November 27, 2018

[†]Department of Chemistry & Biochemistry, Materials Science Institute, University of Oregon, Eugene, Oregon 97403, United States [‡]Department of Physics, Materials Science Institute, Center for Optical, Molecular, and Quantum Science, University of Oregon, Eugene, Oregon 97403, United States

[§]CAMCOR – Center for Advanced Materials Characterization in Oregon, University of Oregon, Eugene, Oregon 97403, United States

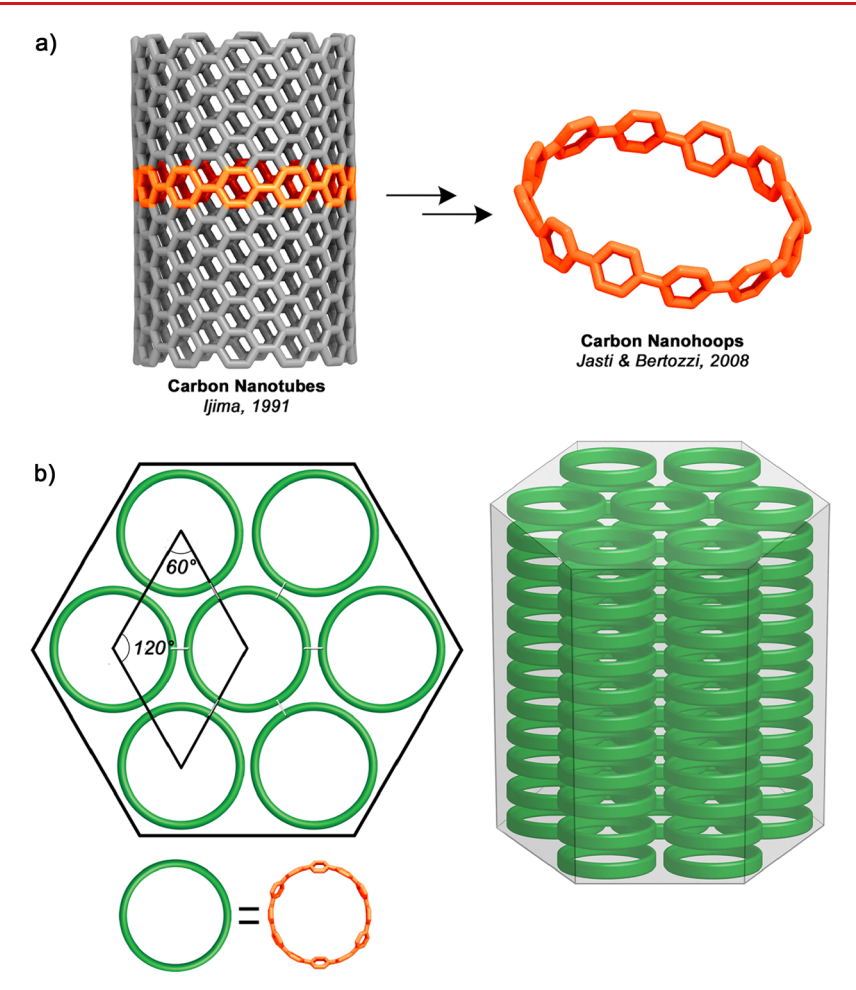


Figure 1. (a) Cartoon representation of a [12,12] armchair CNT and an X-ray crystal structure of its smallest cross-sectional fragment, [12]CPP (crystal structure data from ref 36). (b) (Left) schematic depiction of hexagonal circle packing, in which the central circle in the lattice is symmetrically surrounded by six other circles. CPPs can be seen as geometrically equivalent to perfect circles. (Right) stacking sheets of hexagonally packed hollow circles resulting in the formation of channels with diameters defined by the constituent circles.

Through the vertical self-assembly of CPPs, we speculated that it would be possible to construct arrays of noncovalent nanotubes with diameters that could be synthetically altered with atomic precision. Moreover, the properties of these materials could be fine-tuned via the bottom-up functionalization of nanohoop building blocks. In this work, we merge synthetic organic chemistry, supramolecular design, and fundamental circle packing theory to construct arrays of noncovalent nanotubes with uniform channel diameters of precisely 1.63 nm via the self-assembly of functionalized nanohoop building blocks. We then prepare vertically oriented "forests" of these structures on a highly ordered pyrolytic graphite (HOPG) surface through epitaxial growth using a simple solution-casting approach.

CPPs are unique among macrocyclic small molecules in that their full sp² hybridization and para connectivity gives rise to a circular geometry. Thus, we were curious to what extent CPPs could be treated as geometrically perfect circles, as this would allow for elementary circle packing concepts in our design.³³ Inspired by the dense arrangements found within CNT bundles,³⁴ we ultimately targeted a hexagonal circle packing motif, the densest arrangement for circles of identical diameters.³³ This packing requires each circle in the 2D lattice to be symmetrically surrounded by six other circles (Figure 1b). Stacking these hexagonal "sheets" vertically would then

afford the desired CNT-like columns (Figure 1b). Translating all of this into practical molecular design necessitated a supramolecular strategy that would allow for both face-to-face (horizontal) and edge-to-edge (vertical) interactions between nanohoops. Unfunctionalized CPPs do not exhibit face-to-face arene-arene stacking, as is often observed in linear acene systems³⁵ and instead tend to adopt dense herringbone-like packing motifs with inaccessible pores as a result of the hoops "filling" one another. 27,36 However, arene-perfluoroarene interactions have yet to be thoroughly explored as a selfassembly strategy in CPP systems and were viewed as an attractive alternative to induce the desired face-to-face arrangement. Arene-perfluoroarene interactions, which result from the favorable electronic interaction between electron-rich aryl rings and electron-deficient perfluorinated aryl rings,³ have proven useful in supramolecular design due to their powerful and relatively predictable self-assembly capabilities.^{38,39} Conveniently, aryl C-H···F interactions are also known to be powerful guiding forces in systems containing fluorinated aryl moieties. 40 Therefore, we hypothesized that a drive to maximize C-H···F contacts would "lock" 1 into a vertical assembly.

Nanohoop 1 (Figure 2a) was designed to leverage the symmetry of the [12]CPP backbone to afford six areneperfluoroarene interactions per hoop, where every interaction

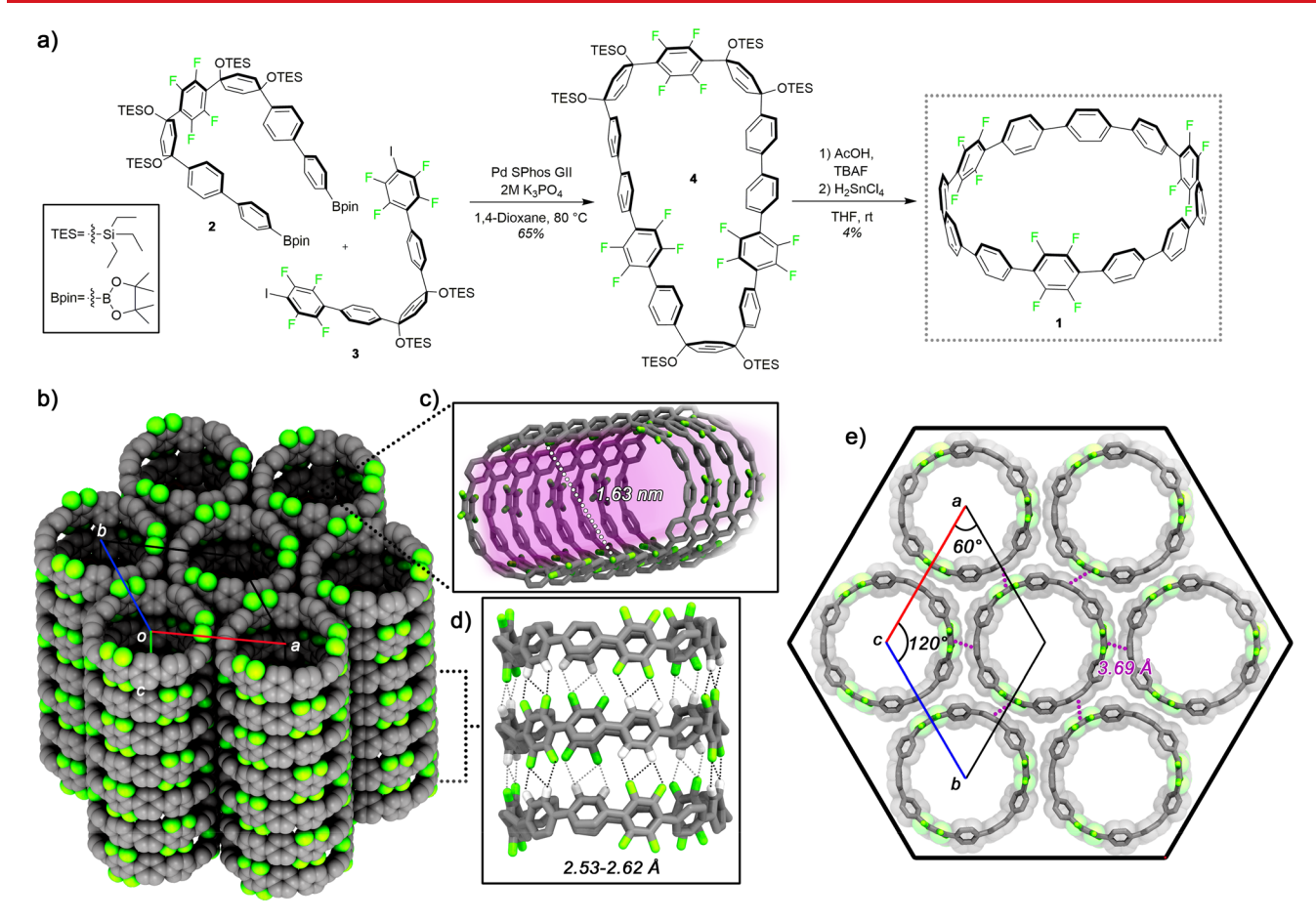


Figure 2. (a) Coupling of intermediates 2 and 3 via Suzuki—Miyaura conditions affords macrocycle 4, which is then deprotected with TBAF and subsequently aromatized under mild tin-mediated conditions to provide fluorinated nanohoop 1. (b) X-ray crystal structure of nanohoop 1, showing that the compound self-assembles into noncovalent nanotubes in the solid state. (c) Cross-section of a nanotube of 1, highlighting the 1.63 nm diameter. (d) Aryl C—H···F interactions (dotted lines) that guide the vertical assembly of 1, which range in distance from 2.53 to 2.62 Å. (e) Top-down view showing the hexagonal circle packing of 1, which is guided by six arene—perfluoroarene interactions that measure at 3.69 Å (purple dotted lines) (chloroform solvent molecules omitted for clarity).

represents one of the six hoop-to-hoop contacts needed to achieve hexagonal packing. Additionally, we hypothesized that C-H···F interactions would align 1 into nanotube-like channels. Yamago and co-workers have recently found that incorporation of fluorines into a nanohoop backbone can indeed result in tubular solid-state structures via fluorinehydrogen interactions.41 The synthesis of 1 relied on previously established synthetic routes toward the size-selective synthesis of [n]CPPs. 17,19 Compounds 2 and 3, which can be easily accessed on a multigram scale (Supporting Information, Schemes S1 and S2), were subjected to a dilute Suzuki-Miyaura cross-coupling reaction, a common aryl-aryl bond forming reaction, ⁴² to afford macrocycle 4 in 65% yield (Figure 2a). Next, the triethylsilyl (TES) groups on the macrocycle were removed with tetrabutylammonium fluoride (TBAF) in the presence of excess acetic acid to afford an intermediate alcohol-functionalized compound. Finally, the cyclohexadiene moieties of this macrocycle were converted to benzene rings via reductive aromatization under mild tin-mediated conditions¹⁹ to afford nanohoop 1 in a 4% yield over two steps as an off-white powder. We attribute this low yield to difficulty in the reductive aromatization step, a problem that also plagued Yamago and co-workers when employing the same aromatization conditions to their syntheses of fluorinated cycloparaphenylenes. 41 Halogenated cycloparaphenylenes have

been calculated to have higher strain energies than their all-hydrocarbon counterparts which could be contributing to the low yields. 43

Nanohoop 1 was found to readily form colorless, needle-like crystals via slow evaporation from chloroform. X-ray diffraction of these crystals revealed that 1 assembles into the desired nanotube-like structures, exhibiting a uniform array of 1.63 nm channels (Figure 2b,c). The vertical assembly of 1 appeared to be guided by a multitude of aryl C-H···F interactions (Figure 2d), resulting in perfectly linear columns. Thirty-six C-H···F interactions per hoop were found in the crystal packing of 1, ranging from 2.53 to 2.62 Å. The ability of the top and bottom "edges" of macrocycles with radially oriented π systems to take part in a large number of weak contacts has been observed previously⁴⁴ and highlights a potential advantage of using nanohoop-like structures to maximize vertical interactions in the construction of molecular crystalline systems. Upon closer inspection of this solid-state packing, we also observed six well-defined arene-perfluoroarene interactions per nanohoop with centroid-to-centroid distances of 3.69 Å (Figure 2e), well within the range of approximately 3.4-3.9 Å commonly observed in other studies. ^{38,39} Importantly, these interactions result in an ideal 2D hexagonal circle packing motif, which is beautifully reflected in the symmetric, diamond-

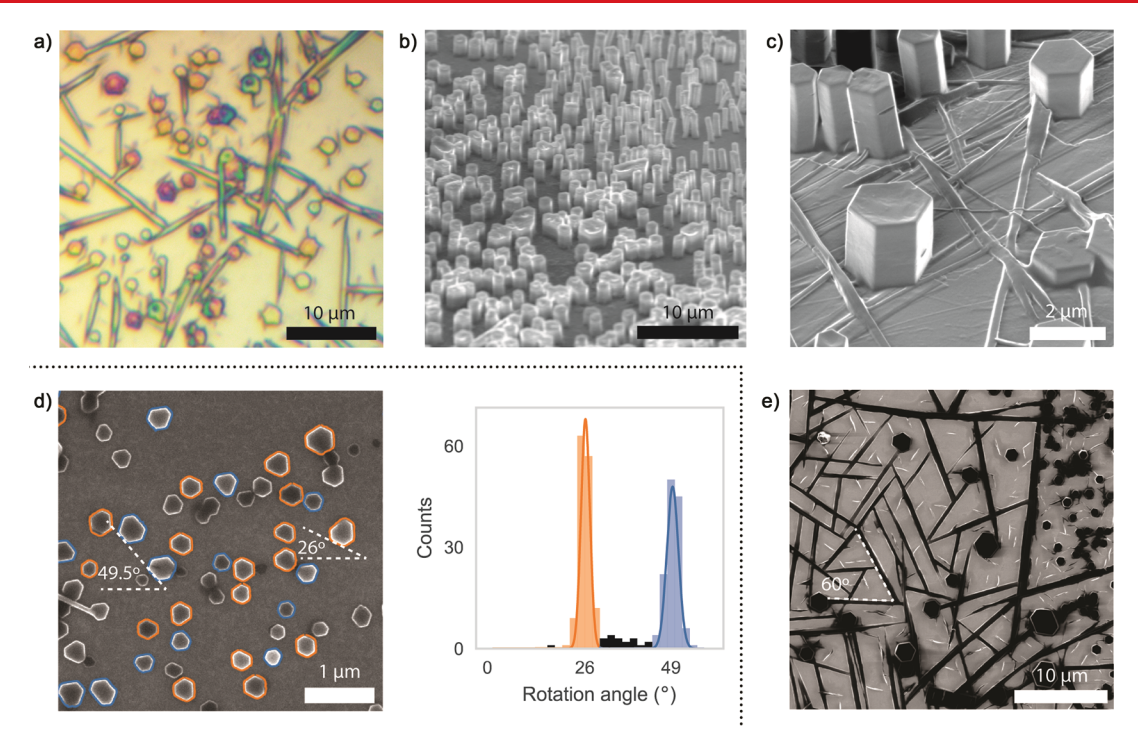


Figure 3. (a) Optical microscopy of hexagonal pillars and needle-like structures on HOPG surface. (b) Angled-SEM of an array of hexagonal pillars. Dense forests of hexagonal pillars are scattered across the sample with heights ranging from a few hundred nanometers to several microns. (c) Angled focused ion beam (FIB) microscopy of isolated hexagonal pillars. The flat hexagonal faces and top are readily apparent. (d) (Left) segment of a larger (25 μ m × 16 μ m) SEM image of short pillars showing growth templated by the substrate. The pillars are preferentially aligned in one of two angles, separated by ~23.5°. (Right) histogram of orientation angles in the full 25 μ m × 16 μ m image. A total of 290 hexagons are identified in the full image and nearly all of them are oriented in one of two angles. (e) FIB image of needle-like structures formed by 1, which preferentially orient at 60° relative to one another on the HOPG surface.

shaped unit cell of the lattice with vertices located at the centers of four nanohoops.

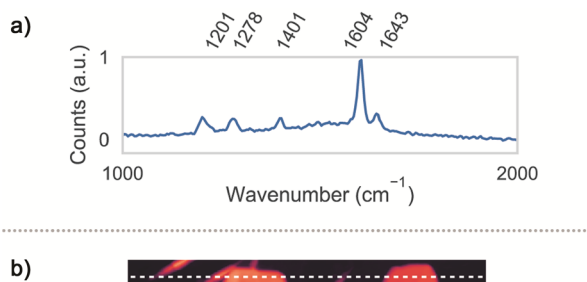
At the outset of this work, one of our primary goals was to mimic vertically oriented CNT "forests" through the vertical assembly of 1 on surfaces. Substrate-templated epitaxial growth has previously been shown to be an effective strategy for accessing well-oriented molecular assemblies.⁴⁵ Thus, we chose highly oriented pyrolytic graphite (HOPG) as a possible template, since HOPG has a lattice constant of a factor of 8 less than the horizontal lattice constants of 1 (a = 2.46 Å for HOPG vs a/b = 19.81 Å for 1). On the basis of this idea of lattice matching, we predicted that HOPG would serve as a suitable template for epitaxial growth of vertically aligned structures of 1. We found that drop-casting 1 from a chloroform solution onto a HOPG substrate at humid ambient conditions (Supporting Information, p S4 and Figure S2) resulted in the rapid ($\sim 1-2$ min) formation of numerous hexagonal and needle-like crystalline structures that were easily observable via optical microscopy (Figure 3a). Scanning electron microscopy (SEM) revealed that the hexagonal crystals were in fact nanowire-like pillars that form dense arrays on many regions of the substrate (Figure 3b). The structures displayed in Figure 3b range in size from 1 to 2 μ m in both height and width, although various other morphologies, such as tall and thin pillars $(5-10 \mu m)$ in height and 0.2-0.5 μ m in width) and short and wide structures (200–500 nm in height and $1-2 \mu m$ in width) were also found (see Supporting Information, Figure S3 for additional images and analysis of the various pillar sizes and morphologies observed). The largest pillars and densest pillar populations were found along the chloroform drying rings that resulted from solution

casting, an observation that could inform future optimization of this solution processing technique. Focused ion beam (FIB) microscopy of individual hexagonal pillars revealed that these structures do indeed exhibit six well-defined walls and a flat hexagonal top (Figure 3c). Satisfyingly, the hexagonal geometries of these pillars directly reflected the hexagonal molecular packing observed in the crystal structure of 1, supporting the notion that the pillars we observed were composed of vertically aligned columns of 1. These pillars were also successfully fabricated on multilayer graphene surfaces grown on copper foil (Figure S4a). It is worth noting that deposition of the nonfluorinated analog ([12]CPP) onto an identical graphene-copper substrate produced no such structures, and instead affords flat plate-like structures consistent with the morphology of solution grown crystals of [12]CPP (Figure S4b).

Further inspection of the hexagonal pillars of 1 revealed preferential orientations on the HOPG surface, which is indicative of epitaxial growth on the graphite lattice. We used a home-built image processing algorithm to identify hexagons and quantify their angles relative to an arbitrary normal. This allowed us to map regions of high pillar density and analyze the relative orientations of grouped pillars. Two distinct orientations for a given area emerged, averaging at 26.0° rotation and 49.5° rotation from an arbitrary normal, which were observed in relatively equal quantities (Figure 3d). We currently hypothesize that these populations represent two energetically favorable orientations that 1 can adopt on the HOPG surface. This notion is supported by a recent theoretical study implying that nanohoops should indeed exhibit energetically preferred orientations on graphene

surfaces.⁴⁶ However, while our findings clearly indicate substrate-directed preferential orientation of the observed hexagonal pillars, further studies are required to elucidate the mechanisms behind the growth and orientation of nanohoop-based structures on graphite. Interestingly, we observe that the needle-like structures align to the graphite surface in multiples of 60° (Figure 3e), consistent with the 3-fold symmetry of the graphite lattice. This again supports the notion that the HOPG surface exhibits a heavy influence on the growth and orientation of the structures formed by 1. Importantly, this well-templated growth offers the potential for deterministic growth of hexagonal wires. For example, a graphene sheet could be patterned into hexagonal growth templates, which would likely facilitate localized growth of pillars.

We used energy-dispersive X-ray spectroscopy (EDS) and Raman spectroscopy to provide additional confirmation that the hexagonal pillars are indeed composed of fluorinated nanohoops. EDS analysis of both pillars and needles produced readily apparent fluorine peaks in addition to carbon (Supporting Information, Figure S5). Solid-state Raman spectroscopy of a single pillar yields a spectrum consistent with previous solution based measurements of cycloparaphenylenes (Figure 4a).⁴⁷ Three previously reported peaks



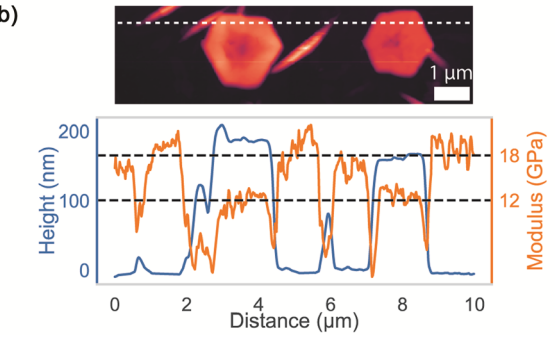


Figure 4. (a) Raman spectrum of a single hexagonal pillar of 1, with peaks observed at 1201, 1278, 1401, 1604, and 1634 cm⁻¹. (b) (Top) PeakForce AFM image of two hexagonal pillars and several needle-like structures. (Bottom) cross-sectional cut of the AFM image (indicated by the dashed white line) showing both the height of the hexagonal pillars (blue) and the elastic modulus (orange).

associated with [12]CPP are observed at 1201 cm⁻¹ (related to C–H bond bending), 1278 cm⁻¹ (attributed to deformation of a benzene ring), and 1604 cm⁻¹ (related to C–C stretching). Two additional peaks, located at 1401 and 1643 cm⁻¹, which have not been seen in CPPs of any diameter, are likely due to the incorporation of fluorine into the atomic structure but could also be due to vibrational modes of the supramolecular crystal. Taken together, the EDS and Raman spectra are consistent with columns of 1 and are in agreement with the atomic structure inferred from X-ray crystallography.

The hexagonal pillars formed by 1 were found to be surprisingly flexible yet mechanically robust. During SEM

imaging, we observed the pillars oscillating like cantilever beams, possibly because of electron-beam-induced electrostatic repulsion between neighboring pillars (see supplementary video). This flexibility is likely a result of the noncovalent assembly of these pillars, demonstrating an inherent utility of a molecular crystalline approach versus assembly methods that involve covalent bond formation. 48 The out-of-plane modulus of the hexagonal pillars, which provides a measure of material stiffness, was found to be similar to those generally observed in molecular crystalline systems. 49 We used PeakForce atomic force microscopy (AFM) to obtain topographical and quantitative nanomechanical images of the pillars (Figure 4b). From this data, we determined that the pillars have an out-of-plane elastic modulus ~12 GPa, about 2/3 that of the HOPG substrate (Figure 4b). The relative flexibility of the vertical nanowires composed of 1, both in- and out-of-plane, suggest that this material can be potentially implemented into flexible devices.50

The bright fluorescence and emission wavelength of the nanohoop building blocks were largely adopted by the hexagonal pillars observed in the solid state. We found the incorporation of fluorine atoms into the backbone of 1 to have little impact on the molecule's photophysical properties in solution, in agreement with the observations of Yamago and co-workers.41 Compared to emission profile of the parent allhydrocarbon [12] CPP in solution,³⁶ the emission profile of 1 is blue-shifted by ~ 10 nm (Figure S4). In the solid state, the fluorescence of 1 is retained and possesses a striking bright blue emission from both the hexagonal pillars and needle-like structures that form following solution deposition onto HOPG (Figure 5a). The emission spectrum of a single-hexagonal pillar reveals two maxima: one at 440 nm, which is also found in solution (Supporting Information, Figure S6), and another lower intensity peak at 480 nm, which is only observed in the solid-state phase (Figure 5b). The absence of the second peak at 480 nm in solution could be due to inhomogeneous broadening,⁵¹ or might be indicative of phonon interactions unique to the solid-state packing of 1. Fluorescence efficiency was found to increase as photon wavelength decreases, before beginning to saturate below 380 nm (Figure 5c), which is consistent with a HOMO-LUMO gap of ~3 eV and falls within the HOMO-LUMO gap range of 2.71-3.63 eV that has been calculated for [5]-[12]CPP. 52 Given how the fluorescence of 1 in solution directly translates to the bulk phase, we expect that the capability to tune CPP properties via size-alteration or functionalization 26,27,53 will allow for the precise tuning of bulk properties in these nanohoop-based materials via the controlled, bottom-up functionalization of nanohoop building blocks.

In conclusion, we have demonstrated the rational design and synthesis of a fluorinated nanohoop (1) that, in the solid state, self-assembles into hexagonally packed bundles of noncovalent nanotubes that bear a striking resemblance to single-walled CNT bundles. Furthermore, vertically aligned "forests" of these hexagonal bundles were constructed on a HOPG substrate via mild solution-casting conditions, which we expect will allow for easy implementation of this material in future solid-state applications. We attribute this preference for vertical growth to the close matching of the respective lattices of 1 and the HOPG surface, which we have supported experimentally via relative angle analysis of both the hexagonal pillars and flatlying needles observed. The hexagonal pillars formed by 1 were further characterized by Raman spectroscopy, AFM imaging,

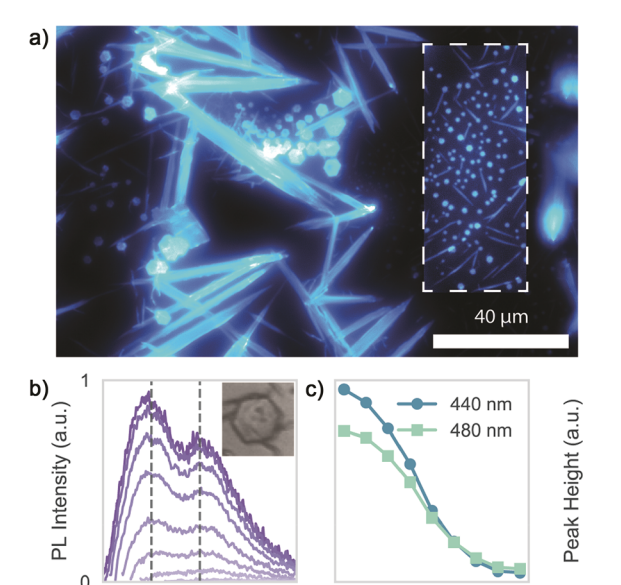


Figure 5. (a) False-colored but visually accurate wide-field fluorescence image of hexagonal pillars and large needle-like structures under UV excitation. The image brightness is enhanced in the boxed region due to the lower fluorescence intensity of the smaller structures within. (b) Emission spectrum at excitation wavelengths ranging from 380 to 420 nm for the single-pillar shown in the inset. Two emission peaks at 440 and 480 nm are apparent for every excitation wavelength. (c) Maximum photoluminescence (PL) intensity from (b) for both the 440 and 480 nm emission maxima peaks as a function of excitation wavelength. The fluorescence efficiency begins to saturate around 380 nm, which is at the limit of our measurement range.

560 380

400

Exc. Wavelength (nm)

400 440

480

Em. Wavelength (nm)

and fluorescence spectroscopy, the latter of which revealed that these pillars retain the bright blue emission exhibited by 1 in solution. The access to precise nanometer-scale channels allowed by this material is expected to be particularly advantageous in highly selective membrane applications. Additionally, unique optical uses are foreseen due to the material's bright emission, which we predict to be synthetically tunable to meet specific needs. More broadly, this study provides an initial blueprint toward the design of self-assembled tubular systems with the potential to mimic the channel environments found within CNTs, albeit with significantly greater control over channel diameter. We also intend to explore this strategy as a means of preorganizing molecular precursors for the precise bottom-up synthesis of CNTs and other extended carbon nanostructures.

ASSOCIATED CONTENT

S Supporting Information

The Supporting Information is available free of charge on the ACS Publications website at DOI: 10.1021/acs.nanolett.8b03979.

Synthetic schemes for intermediates 2 and 3, synthetic procedures, ¹H NMR, ¹³C NMR, ¹⁹F NMR, and mass spectrometry analysis of synthesized compounds, absorption and emission data for 1 in solution, preparation of solid-state samples of 1, SEM images of 1 and [12]CPP on graphene-copper substrate, EDS data, X-ray crystallography data, solid-state characterization

procedures, SEM images of various pillar sizes and morphologies (PDF)
SEM video of pillar oscillation (MPG)

AUTHOR INFORMATION

Corresponding Authors

*B. Alemán. E-mail: baleman@uoregon.edu.

*R. Jasti. E-mail: rjasti@uoregon.edu.

ORCID ®

Jeff M. Van Raden: 0000-0002-3505-5170 David Miller: 0000-0001-5999-1038 Ramesh Jasti: 0000-0002-8606-6339

Author Contributions

E.J.L., J.M.V., and R.J. conceived of the self-assembly of fluorinated CPPs and developed the synthetic methodology to prepare nanohoop 1. Solid-state characterization was carried out by D.M. and B.A. L.N.Z. performed the X-ray crystallographic analysis of 1. The manuscript was written through contributions of all authors. All authors have given approval to the final version of the manuscript.

Notes

The authors declare no competing financial interest.

ACKNOWLEDGMENTS

We acknowledge the facilities and staff from the Center for Advanced Materials in Oregon (CAMCOR) and the use of the University of Oregon's Rapid Materials Prototyping facility, funded by the Murdock Charitable Trust. The synthesis and structural analysis of 1 was supported by the National Science Foundation (NSF) under grant numbers CHE-1808791 and CHE-1800586. Mass spectroscopy support was provided by NSF number CHE-1625529. Solid-state characterization was supported under NSF grant numbers CHE-1531189 and DMR-1532225. All work herein was supported by the University of Oregon.

REFERENCES

- (1) Jariwala, D.; Sangwan, V. K.; Lauhon, L. J.; Marks, T. J.; Hersam, M. C. Chem. Soc. Rev. 2013, 42, 2824–2860.
- (2) Wang, H.; Wang, B.; Quek, X.-Y.; Wei, L.; Zhao, J.; Li, L.-J.; Chan-Park, M. B.; Yang, Y.; Chen, Y. J. Am. Chem. Soc. **2010**, 132, 16747–16749.
- (3) He, M.; Chernov, A. I.; Fedotov, P. V.; Obraztsova, E. D.; Rikkinen, E.; Zhu, Z.; Sainio, J.; Jiang, H.; Nasibulin, A. G.; Kauppinen, E. I.; Niemelä, M.; Krause, A. O. I. *Chem. Commun.* **2011**, 47, 1219–1221.
- (4) Sanchez-Valencia, J. R.; Dienel, T.; Gröning, O.; Shorubalko, I.; Mueller, A.; Jansen, M.; Amsharov, K.; Ruffieux, P.; Fasel, R. *Nature* **2014**, *512*, 61–64.
- (5) Holt, J. K.; Park, H. G.; Wang, Y.; Stadermann, M.; Artyukhin, A. B.; Grigoropoulos, C. P.; Noy, A.; Bakajin, O. *Science* **2006**, *312*, 1034–1037.
- (6) Tunuguntla, R. H.; Allen, F. I.; Kim, K.; Belliveau, A.; Noy, A. Nat. Nanotechnol. **2016**, 11, 639-644.
- (7) Hata, K.; Futaba, D. N.; Mizuno, K.; Namai, T.; Yumura, M.; Iijima, S. Science **2004**, 306, 1362–1364.
- (8) Fornasiero, F.; Park, H. G.; Holt, J. K.; Stadermann, M.; Grigoropoulos, C. P.; Noy, A.; Bakajin, O. *Proc. Natl. Acad. Sci. U. S. A.* **2008**, *105*, 17250–17255.
- (9) Qu, L.; Vaia, R. A.; Dai, L. ACS Nano 2011, 5, 994-1002.
- (10) Bsoul, A.; Sultan Mohamed Ali, M.; Nojeh, A.; Takahata, K. Appl. Phys. Lett. **2012**, 100, 213510.
- (11) Miyake, T.; Yoshino, S.; Yamada, T.; Hata, K.; Nishizawa, M. J. Am. Chem. Soc. 2011, 133, 5129-5134.

(12) Smalley, R. E.; Li, Y.; Moore, V. C.; Price, B. K.; Colorado, R.; Schmidt, H. K.; Hauge, R. H.; Barron, A. R.; Tour, J. M. *J. Am. Chem. Soc.* **2006**, *128*, 15824–15829.

- (13) Xia, J.; Golder, M. R.; Foster, M. E.; Wong, B. M.; Jasti, R. J. Am. Chem. Soc. **2012**. 134. 19709—19715.
- (14) Sisto, T. J.; Tian, X.; Jasti, R. J. Org. Chem. 2012, 77, 5857–5860.
- (15) Omachi, H.; Nakayama, T.; Takahashi, E.; Segawa, Y.; Itami, K. Nat. Chem. **2013**, *5*, 572–576.
- (16) Jasti, R.; Bhattacharjee, J.; Neaton, J. B.; Bertozzi, C. R. J. Am. Chem. Soc. **2008**, 130, 17646–17647.
- (17) Darzi, E. R.; Sisto, T. J.; Jasti, R. J. Org. Chem. **2012**, 77, 6624–6628.
- (18) Xia, J.; Jasti, R. Angew. Chem., Int. Ed. 2012, 51, 2474-2476.
- (19) Patel, V. K.; Kayahara, E.; Yamago, S. Chem. Eur. J. 2015, 21, 5742–5749.
- (20) Evans, P. J.; Darzi, E. R.; Jasti, R. Nat. Chem. 2014, 6, 404-408.
- (21) Tran-Van, A.-F.; Huxol, E.; Basler, J. M.; Neuburger, M.; Adjizian, J.-J.; Ewels, C. P.; Wegner, H. A. *Org. Lett.* **2014**, *16*, 1594–1597.
- (22) Van Raden, J. M.; Louie, S.; Zakharov, L. N.; Jasti, R. J. Am. Chem. Soc. 2017, 139, 2936–2939.
- (23) White, B. M.; Zhao, Y.; Kawashima, T. E.; Branchaud, B. P.; Pluth, M. D.; Jasti, R. ACS Cent. Sci. 2018, 4, 1173–1178.
- (24) Povie, G.; Segawa, Y.; Nishihara, T.; Miyauchi, Y.; Itami, K. Science 2017, 356, 172-175.
- (25) Povie, G.; Segawa, Y.; Nishihara, T.; Miyauchi, Y.; Itami, K. J. Am. Chem. Soc. **2018**, 140, 10054–100059.
- (26) Fujitsuka, M.; Cho, D. W.; Iwamoto, T.; Yamago, S.; Majima, T. Phys. Chem. Chem. Phys. **2012**, *14*, 14585–14588.
- (27) Darzi, E. R.; Jasti, R. Chem. Soc. Rev. 2015, 44, 6401-6410.
- (28) Sakamoto, H.; Fujimori, T.; Li, X.; Kaneko, K.; Kan, K.; Ozaki, N.; Hijikata, Y.; Irle, S.; Itami, K. Chem. Sci. **2016**, 7, 4204–4210.
- (29) Kayahara, E.; Sun, L.; Onishi, H.; Suzuki, K.; Fukushima, T.; Sawada, A.; Kaji, H.; Yamago, S. *J. Am. Chem. Soc.* **2017**, *139*, 18480–18482
- (30) Ozaki, N.; Sakamoto, H.; Nishihara, T.; Fujimori, T.; Hijikata, Y.; Kimura, R.; Irle, S.; Itami, K. *Angew. Chem., Int. Ed.* **2017**, *56*, 11196–11202.
- (31) Mori, T.; Tanaka, H.; Dalui, A.; Mitoma, N.; Suzuki, K.; Matsumoto, M.; Aggarwal, N.; Patnaik, A.; Acharya, S.; Shrestha, L. K.; Sakamoto, H.; Itami, K.; Ariga, K. *Angew. Chem., Int. Ed.* **2018**, *57*, 9679–9683.
- (32) Ball, M.; Zhong, Y.; Fowler, B.; Zhang, B.; Li, P.; Etkin, G.; Paley, D. W.; Decatur, J.; Dalsania, A. K.; Li, H.; Xiao, S.; Ng, F.; Steigerwald, M. L.; Nuckolls, C. *J. Am. Chem. Soc.* **2016**, *138*, 12861–12867.
- (33) Bezdek, A.; Kuperberg, W. Mathematika 1990, 37, 74-80.
- (34) Peigney, A.; Laurent, C.; Flahaut, E.; Bacsa, R. R.; Rousset, A. Carbon 2001, 39, 507-514.
- (35) Anthony, J. E.; Brooks, J. S.; Eaton, D. L.; Parkin, S. R. J. Am. Chem. Soc. **2001**, 123, 9482–9483.
- (36) Segawa, Y.; Miyamoto, S.; Omachi, H.; Matsuura, S.; Šenel, P.; Sasamori, T.; Tokitoh, N.; Itami, K. *Angew. Chem., Int. Ed.* **2011**, *50*, 3244–3248.
- (37) Patrick, C. R.; Prosser, G. S. Nature 1960, 187, 1021.
- (38) Coates, G. W.; Dunn, A. R.; Henling, L. M.; Dougherty, D. A.; Grubbs, R. H. *Angew. Chem., Int. Ed. Engl.* **1997**, *36*, 248–251.
- (39) Kissel, P.; Murray, D. J.; Wulftange, W. J.; Catalano, V. J.; King, B. T. *Nat. Chem.* **2014**, *6*, 774–778.
- (40) Thalladi, V. R.; Weiss, H.-C.; Bläser, D.; Boese, R.; Nangia, A.; Desiraju, G. R. *J. Am. Chem. Soc.* **1998**, *120*, 8702–8710.
- (41) Hashimoto, S.; Kayahara, E.; Mizuhata, Y.; Tokitoh, N.; Takeuchi, K.; Ozawa, F.; Yamago, S. Org. Lett. 2018, 20, 5973–5976.
- (42) Suzuki, A. Angew. Chem., Int. Ed. 2011, 50, 6722-6737.
- (43) Rio, J.; Erbahar, D.; Rayson, M.; Briddon, P.; Ewels, C. P. Phys. Chem. Chem. Phys. **2016**, 18, 23257–23263.
- (44) Li, P.; Zakharov, L. N.; Jasti, R. Angew. Chem., Int. Ed. 2017, 56, 5237–5241.

(45) Falcaro, P.; Okada, K.; Hara, T.; Ikigaki, K.; Tokudome, Y.; Thornton, A. W.; Hill, A. J.; Williams, T.; Doonan, C.; Takahashi, M. *Nat. Mater.* **2017**, *16*, 342–348.

- (46) Pérez-Guardiola, A.; Pérez-Jiménez, A. J.; Sancho-García, J. C. Mol. Syst. Des. Eng. 2017, 2, 253.
- (47) Chen, H.; Golder, M. R.; Wang, F.; Jasti, R.; Swan, A. K. Carbon 2014, 67, 203–213.
- (48) Cooper, A. I. ACS Cent. Sci. 2017, 3, 544-553.
- (49) Tan, J. C.; Cheetham, A. K. Chem. Soc. Rev. 2011, 40, 1059-
- (50) Beaujuge, P. M.; Fréchet, J. M. J. J. Am. Chem. Soc. 2011, 133, 20009-20029.
- (51) Valeur, B. *Molecular Fluorescence*; Wiley-VCH Verlag GmbH & Co. KGaA: Weinheim, Germany, 2001.
- (52) Iwamoto, T.; Watanabe, Y.; Sakamoto, Y.; Suzuki, T.; Yamago, S. J. Am. Chem. Soc. **2011**, 133, 8354–8361.
- (53) Kuwabara, T.; Orii, J.; Segawa, Y.; Itami, K. Angew. Chem., Int. Ed. 2015, 54, 9646–9649.